npj | Computational Materials

www.nature.com/npjcompumats

ARTICLE OPEN

Revisiting the anchoring behavior in lithium-sulfur batteries: many-body effect on the suppression of shuttle effect

Min Fang[1], Xinyi Liu[1], Ji-Chang Ren[1], Sha Yang[1], Guirong Su[1], Qin Fang[1], Jianzhong Lai[2], Shuang Li[1*] and Wei Liu[1*]

We apply the state-of-the-art many-body dispersion (MBD) method to study the anchoring behavior in lithium-sulfur (Li–S) batteries, which is closely related to the notorious "shuttle effect". Based on the experimental results of metal sulfides (FeS and SnS_2), we find that the MBD method gives a more accurate prediction of anchoring mechanism compared with other van der Waals (vdW) inclusive methods. We systematically investigate the anchoring mechanism of two prototypal anchoring materials—Ti_2CF_2 and doped-graphene systems. The many-body effect is found to play an important role on the reduction of anchoring behaviors, especially when the systems have large polarization and the vdW interactions predominate the anchoring behavior. Our work deepens the fundamental understanding of the anchoring mechanism, and provides a more accurate criterion for screening anchoring materials for suppressing the shuttle effect.

npj Computational Materials (2020)6:8 ; https://doi.org/10.1038/s41524-020-0273-1

INTRODUCTION

Lithium-sulfur batteries (Li–S) fulfill the urgent demands on the storage and transport of renewable energy, owing to their overwhelming theoretical energy density and relatively low cost.[1–7] However, one of the fatal issues that restricts the commercialization of Li–S batteries is the notorious "shuttle effect", which stems from the dissolution and the endless transport/shuttle of lithium polysulfides (LiPSs) between cathode and anode during the redox process. These phenomena greatly reduce the utilization of sulfur and Coulomb efficiency, causing the self-discharge behavior and the rapid decrease of battery capacity.[8] For the practical applications of Li–S batteries, the shuttle effect has to be greatly suppressed in liquid electrolyte.[9]

An effective strategy for overcoming the shuttle effect is to introduce anchoring materials in cathode to trap LiPSs. Conductive mesoporous carbon framework was first used to encapsulate the sulfur cathode.[10] Subsequently, functionalized carbon materials were developed to enhance the polarity of carbon materials.[11] Recently, two-dimensional (2D) materials like polar metallic oxides,[12,13] transition-metal sulfides,[14] and metal nitrides,[15] were utilized to alleviate the shuttle effect, but their applications are limited by their bad conductivity. Encouragingly, 2D transition-metal carbides, carbonitrides, and nitrides (known as MXenes)[16] have been demonstrated to greatly promote the electrochemical performance for energy storage devices.[17–20] Because of their prominent advantages, such as metallic conductivity, a plastic layer structure, and the hydrophilic nature of its functionalized surface,[21] MXenes have been intensively investigated as anchoring materials in Li–S batteris.[22–24]

The accurate prediction of binding energies between anchoring materials, electrolytes, and LiPSs is a prerequisite for uncovering the anchoring mechanism and design cathode in Li–S batteries.[25–27] In this contribution, we apply the many-body dispersion (MBD) method to investigate two prototypal anchoring materials and find that the many-body effect significantly affects the binding energies of LiPSs on Ti_2CF_2. In this system the larger many-body effect originates from the large polarization and the domination of van der Waals (vdW) forces. In contrast, for N-doped graphene (NG) systems, the contribution of the many-body effect for binding strength is only 2%, since the chemical bonding predominates the whole process of lithiation. Our work paves the way for more reliably screening anchoring materials to control the shuttle effect and to design high-performance cathode materials for Li–S batteries.

RESULTS

Performance of FeS and SnS_2 for trapping Li_2S_6

Zhou et al.[28] have experimentally investigated the anchoring behavior of metal sulfides for trapping Li_2S_6 by comparative tests (different metal sulfides with equivalent total surface area were added into originally yellow-colored 1, 2-dimethoxyethane/1, 3-dioxolane (DME/DOL) solution with Li_2S_6). According to the discoloration of solution, they found that the metal sulfides have different adsorption capability for Li_2S_6 and several of them completely suppressed the shuttle effect. The competition between anchoring materials and electrolytes for trapping soluble LiPSs has been concerned to evaluate anchoring materials.[29,30] However, in their density functional theory (DFT) calculation the anchoring factor ΔE ($\Delta E = E^b_{AM} - E^b_{so}$) was not considered. Here E^b_{AM} is the binding energies of LiPSs absorbed on anchoring materials, and E^b_{so} denotes the binding energies of LiPSs with electrolyte molecules. The positive ΔE indicates that the interaction between polysulfides and anchoring materials is stronger than polysulfides with electrolyte molecules; the negative ΔE means that polysulfides tend to dissolve into electrolyte rather than absorb on anchoring materials.

To compare theoretical prediction from different vdW methods, we apply a criterion (ΔE) to evaluate the performance of FeS and SnS_2 for trapping Li_2S_6 and compare with experimental observation.[28] The optimized configurations of Li_2S_6 absorbed on FeS and SnS_2, and its binding with DME/DOL molecule are shown in Supplementary Fig. 1. Recently, Brandenburg et al.[31] reported that the MBD method performs better than most other approaches,

[1]Nano and Heterogeneous Materials Center, Nanjing University of Science and Technology, Nanjing 210094, China. [2]School of Materials Science and Engineering, Nanjing University of Science and Technology, Nanjing 210094, China. *email: lishuang@njust.edu.cn; weiliu@njust.edu.cn

Table 1. The binding energies (eV) between Li_2S_6 and anchoring materials (FeS and SnS_2) as well as electrolyte molecules (DME and DOL) from several DFT methods, the anchoring factor ΔE are also listed.

Li_2S_6	PBE + MBD	PBE + vdW^{surf}	PBE + D2	PBE + D3	vdW-DF2	optB86b-vdW
FeS	0.84	1.31	0.88	1.02	1.37	1.02
SnS_2	0.87	1.06	0.79	0.96	1.27	0.94
DME	0.94	0.83	0.94	0.84	0.94	0.83
DOL	0.82	0.77	0.84	0.78	0.91	0.74
ΔE (FeS-DME)	−0.10	0.48	−0.06	0.18	0.43	0.19
ΔE (FeS-DOL)	0.02	0.54	0.04	0.24	0.46	0.28
ΔE (SnS_2-DME)	−0.07	0.23	−0.15	0.12	0.33	0.11
ΔE (SnS_2-DOL)	0.05	0.29	−0.05	0.18	0.36	0.20

Summary of the binding energies and anchoring factor from several DFT methods

such as DMC and CCSD(T), for the fundamental system. Meanwhile, it has been demonstrated that it is essential to include the many-body effect in adsorption systems for the evaluation of binding energies.[32–34] In this context, here we apply the MBD method to predict the interaction between Li_2S_6 and FeS/SnS_2. From the results of PBE + MBD method in Table 1, Δ*E* (FeS-DME) and Δ*E* (SnS_2-DME) are negative values (−0.10 eV and −0.07 eV), Δ*E* (FeS-DOL) and Δ*E* (SnS_2-DOL) are positive values (0.02 eV and 0.05 eV). We predict that a part of Li_2S_6 species will be anchored on the surface of FeS and SnS_2 and the rest of Li_2S_6 still binds with DME molecules. In other words, the yellow DME/DOL solution with Li_2S_6 just has an incompletely discoloration when FeS and SnS_2 are added as anchoring materials. This conclusion is fully compatible with the experimental observation.

However, from the PBE + D2 method, the Δ*E* (FeS-DOL) is 0.04 eV and other Δ*E* values are negative, which suggests that SnS_2 cannot trap Li_2S_6 species efficiently. Therefore, the yellow DME/DOL solution with Li_2S_6 should keep the color invariable when SnS_2 is used as anchoring materials. From the PBE + vdW^{surf}, PBE + D3, vdW-DF2 and optB86b-vdW methods, all Δ*E* are positive values, implying that Li_2S_6 is absorbed on FeS and SnS_2 firmly and scarcely binds with DME/DOL molecules. Thus, the yellow DME/DOL solution with Li_2S_6 should fade completely. Nevertheless, the experiment clearly showed that when FeS and SnS_2 are added as anchoring materials, the originally yellow-colored polysulfide solution becomes lighter in color rather than become colorless in experimental observation. Therefore, the conclusion from those computational methods is inconsistent with experimental observation.

Performance of Ti_2CF_2 and NG for trapping LiPSs

According to the above analysis, the MBD method is more accurate than other methods to describe the interaction between LiPSs and metal sulfides. However, many studies also got reasonable conclusions of the anchoring materials for suppression of the shuttle effect by pairwise-based methods.[26,30,35] Therefore, to attain an in-depth understanding of the many-body effect on binding strength of LiPSs with anchoring materials, we selected Ti_2CF_2 and NG as platforms and investigated their intrinsic different anchoring mechanisms. Ti_2C-based materials are the lightest Mxenes and atom-multilayered 2D materials, NG is a typical heteroatom-doped anchoring material with one-atomic-layer structure. As for Ti_2CF_2, we note that the F-termination has different adsorption sites on Ti_2C surface[36,37] and the HCP site is chosen in our work because of the stronger binding strength of LiPSs (Supplementary Fig. 2 and Supplementary Table 1). Firstly, the configurations of soluble LiPSs with electrolyte molecules are investigated. Notably, the real electrolyte system is very complicated, which usually consists of solvents, lithium salts, and additives.[38] Nevertheless, the major component causing the shuttle effect is solvent molecules in electrolyte, which competes with anchoring materials and introduces solution of high-order LiPSs. As such, in the present work, and the same in previous work,[29,30] we used DME and DOL molecules to explain the interaction between LiPSs and electrolyte. We considered that one LiPSs cluster interacts with one or two DME (DOL) molecules (Supplementary Fig. 3). From Supplementary Table 2 we find that the E^b_{so} are very similar whatever soluble LiPSs binding with one or two DME (DOL) molecules from the vdW^{surf} and MBD methods. For systematically examining the E^b_{AM} between LiPSs and Ti_2CF_2/NG, various initial adsorption configurations of Li_2S_n ($n = 1, 2, 4, 6,$ and 8) clusters are considered to find the optimized structures. The most stable structures with the lowest energy are shown in Fig. 1a. Comparing with Li_2S_6 and Li_2S_8, Li_2S, Li_2S_2, and Li_2S_4 prefer to adsorb vertically on Ti_2CF_2, with two Li atoms binding with Ti_2CF_2. We also search the most stable configurations in NG systems (Supplementary Fig. 4). The calculated E^b_{AM} of most stable configurations from PBE + vdW^{surf}, PBE + MBD, and other methods at different lithiation stages are shown in Table 2, Fig. 2a, b, and Supplementary Table 3.

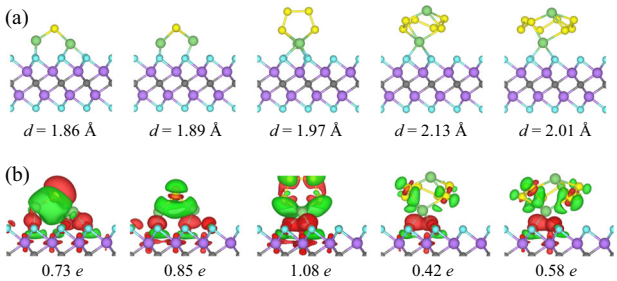

Fig. 1 The adsorption configurations and charge transfers of LiPSs adsorbed on Ti_2CF_2. **a** Side views of the most stable configurations of Li_2S_n ($n = 1, 2, 4, 6, 8$) anchoring on Ti_2CF_2. The shortest length of Li–S bond is also labeled. **b** Charge transfers between LiPSs and Ti_2CF_2. Here, red (green) is the spatial regions gain (loss) in charge. In all configurations LiPSs lose charge and Ti_2CF_2 obtain charge. The value of charge transfer is labeled. The purple, gray, sky blue, yellow, and green spheres represent the Ti, C, F, S, and Li atoms, respectively.

Figure 2a shows that the PBE + MBD method reduces the E^b_{AM} over 20% compared to the PBE + vdW^{surf} method at high-order lithiation stages for Ti_2CF_2 systems. In contrast, the binding energies for the NG systems from the two methods are almost identical (Fig. 2b). To assess the contribution of MBD to the E^b_{AM}, we determine the ratio of MBD contribution (R_{MBD}) as follows,

$$R_{MBD} = (E^b_{vdW} - E^b_{MBD})/E^b_{MBD} \quad (1)$$

Table 2. Computed binding energies (eV) between LiPSs and Ti_2CF_2/NG from the PBE + vdW^{surf} and PBE + MBD methods.

	Ti_2CF_2					NG				
	PBE + vdW^{surf}	PBE + MBD	R_{MBD}	R_{vdW}	ΔE_{MBD}	PBE + vdW^{surf}	PBE + MBD	R_{MBD}	R_{vdW}	ΔE_{MBD}
Li_2S	2.36	2.02	16.8	53.5	–	2.76	2.80	1.4	17.9	–
Li_2S_2	2.14	1.86	15.1	59.1	–	2.85	2.81	1.4	23.1	–
Li_2S_4	1.61	1.24	29.8	99.2	0.34	2.33	2.33	0.0	34.8	1.43
Li_2S_6	1.28	0.96	33.3	110.4	0.02	2.37	2.34	1.3	41.9	1.40
Li_2S_8	1.51	1.20	25.8	105.0	0.24	2.63	2.65	0.8	44.9	1.69

Summary of the binding energies, ratio for the many-body effect and vdW interaction in Ti_2CF_2 and NG systems
R_{MBD} (%) and R_{vdW} (%) is the ratio for the many-body effect and vdW interaction of binding energies. ΔE_{MBD} ($\Delta E_{MBD} = E^b_{AM} - E^b_{DME}$) is the anchoring factor of high-order LiPSs from the PBE + MBD method

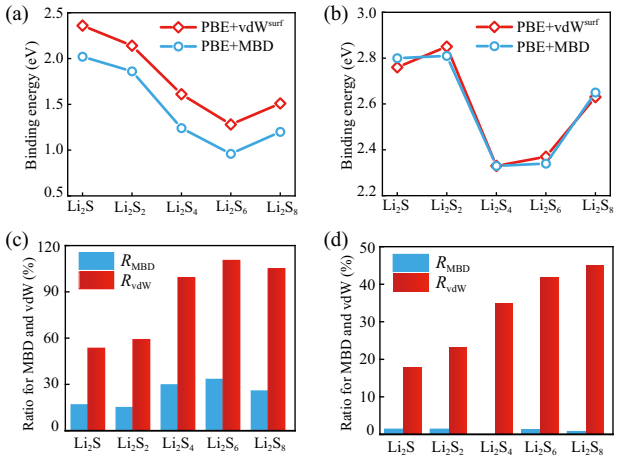

Fig. 2 The binding energies and ratio for many-body effect and vdW interaction of Ti_2CF_2 and NG systems. Computed binding energies for **a** LiPSs on Ti_2CF_2 and **b** LiPSs on NG with the PBE + vdW^{surf} and PBE + MBD methods. The ratio for many-body effect (R_{MBD}) and vdW interaction (R_{vdW}) of binding energies in (**c**) Ti_2CF_2 systems and **d** NG systems.

where E^b_{vdW} and E^b_{MBD} denote the binding energies of Ti_2CF_2 (NG) from the PBE + vdW^{surf} and PBD + MBD methods, respectively. The magnitudes of R_{MBD} for LiPSs absorbed on Ti_2CF_2 and NG are shown in Fig. 2c, d. From Table 2, when Ti_2CF_2 are selected as anchoring materials, we find that R_{MBD} varies from 16.8% to 33.3% with the delithiation of LiPSs. The many-body effect affects Li_2S_6-Ti_2CF_2 system largely, which has weakened the binding strength by 33.3% and may lead to the dissolution of Li_2S_6 due to the small ΔE (0.02 eV). While for the NG system, we find that the R_{MBD} (range from 0 to 1.4%) is slight and the many-body effect could be ignored.

To attain an in-depth understanding why the MBD method reduces the binding strength of LiPSs with anchoring materials, we divide the E^b_{AM} into two aspects: the vdW part corresponds to the physical interaction, and the PBE part (termed as E^b_{PBE}) corresponds to the chemical interaction using pairwise-based method vdW^{surf}, because the MBD effect mainly contributes to the part of physical interaction. To clarify how these two aspects affect the anchoring behavior, we define the ratio of the vdW interaction (R_{vdW}) as follows,

$$R_{vdW} = (E^b_{vdW} - E^b_{PBE})/E^b_{vdW} \quad (2)$$

In Eq. (2), E^b_{vdW} denotes E^b_{AM} from the pairwise PBE + vdW^{surf} method. The ratio of vdW contribution to E^b_{AM} for Ti_2CF_2 systems is shown in Fig. 2c, the vdW interaction shows different weights towards different lithiation stages. During the delithiation from Li_2S to Li_2S_8, the Li-F bond length increases from 1.86 to 2.01 Å, suggesting that the chemical interaction is gradually weakened. The bond length is 1.86 and 1.88 Å for Li_2S and Li_2S_2 absorbed on Ti_2CF_2 (within the distances of covalent bonds), and the R_{vdW} is 53% and 59%, respectively. This suggests that both chemical interaction and vdW interactions play important roles in these two adsorption systems. However, the physical interaction dominates the E^b_{AM} of high-order Li_2S_n species ($n = 4, 6, 8$) absorbed on Ti_2CF_2 (the R_{vdW} nearly 100%). In contrast, although the R_{vdW} for the NG systems increases with the increasing size of LiPSs, the R_{vdW} of NG systems (ranges from 18% to 45%) is smaller than those of Ti_2CF_2 systems especially for high-order LiPSs, so the chemical interaction (the bond length of Li-N ranges from 1.86 Å to 1.90 Å) dominates the whole process of lithiation (Fig. 2d).

Static polarizability of adsorption systems and charge transfer

Comparing with pairwise vdW-correction methods, the MBD method computes the correlation energy of long-range electrostatic screening through the coupled harmonic oscillator model Hamiltonian, and considers dipolar vdW interactions to all orders in perturbation theory.[39] The reduction of E^b_{AM} from the PBE + MBD method must come from the collective inclusion of the long-range electrostatic screening. Polarizability is central to the description of the long-range electron correlation, which indicates the willingness of a material to respond under the influence of a perturbation of the electric field. It is known that five atomic layers of Ti_2CF_2 are stacked along the *c*-axis direction, middle Ti atoms experience the dynamic electric field created by the upper and lower atoms, which gives rise to polarization effects.[40] To provide a quantitative description of the polarizability, we define the changes in static polarizability of the adsorption systems $\Delta\alpha$ by

$$\Delta\alpha = \Delta\alpha_{total} - \Delta\alpha_{AM} - \Delta\alpha_{LiPSs} \quad (3)$$

where $\Delta\alpha_{total}$, $\Delta\alpha_{AM}$, and $\Delta\alpha_{LiPSs}$ represent the screened static polarizabilities of the adsorption systems, the anchoring materials and the free-standing LiPSs, respectively. Considering the similar polarizabilities along *x* and *y* coordinates, we present the $\Delta\alpha$ along *x* and *z* directions, termed as $\Delta\alpha_{\parallel}$ and $\Delta\alpha_{\perp}$, which are parallel and perpendicular to the surface of 2D anchoring materials, respectively. The calculated $\Delta\alpha$ ($\Delta\alpha_{\parallel}$ and $\Delta\alpha_{\perp}$) are listed in Table 3. We find that for Ti_2CF_2 systems, contrary to the magnitude of $\Delta\alpha_{\parallel}$ that varies slightly, the magnitudes of $\Delta\alpha_{\perp}$ are very different from the delithiation of LiPSs. We find that $\Delta\alpha_{\perp}$ are positive for Ti_2CF_2 systems, which means that the adsorption of LiPSs increases the $\Delta\alpha_{\perp}$ of the systems. However, the values of $\Delta\alpha_{\perp}$ in N-doped graphene adsorption systems are negative, indicating that the $\Delta\alpha_{\perp}$ are decreased after LiPSs adsorbed on N-doped graphene.

We notice that the magnitudes of $\Delta\alpha_{\perp}$ of Li_2S_6 and Li_2S_8 absorbed on Ti_2CF_2 decrease to 10 $bohr^3$. The decreasing values of $\Delta\alpha_{\perp}$ suggest the weakening of the polarization along

Table 3. The total static polarizability ($\Delta\alpha$), and the $\Delta\alpha$ along x ($\Delta\alpha_{\parallel}$) and z ($\Delta\alpha_{\perp}$) directions of Ti_2CF_2 adsorption configurations.

Ti_2CF_2	Li_2S	Li_2S_2	Li_2S_4	Li_2S_6	Li_2S_8
$\Delta\alpha$(bohr^3)	33.7	41.3	37.2	22.7	22.2
$\Delta\alpha_{\parallel}$(bohr^3)	52.1	51.2	54.2	51.4	48.3
$\Delta\alpha_{\perp}$(bohr^3)	32.7	52.8	48.9	10.5	9.6
Q (e)	0.73	0.85	1.08	0.42	0.58
NG	Li_2S	Li_2S_2	Li_2S_4	Li_2S_6	Li_2S_8
$\Delta\alpha$(bohr^3)	4.3	5.7	12.0	11.9	11.0
$\Delta\alpha_{\perp}$(bohr^3)	−7.4	−9.2	−20.3	−12.1	−14.7
Q (e)	0.67	0.75	0.55	0.36	0.38

Summary of the static polarizability and charge transfer in Ti_2CF_2 and NG systems
The charge transfer (Q) between LiPSs and Ti_2CF_2(NG) are also shown in the table

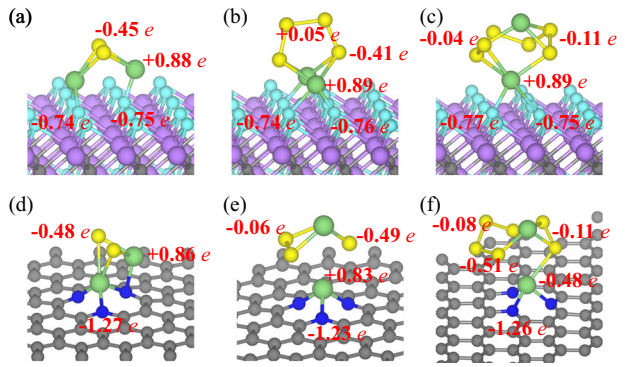

Fig. 3 Charge distribution analysis of LiPSs adsorbed on Ti_2CF_2 and NG. a–c The charge transfers (e) of S and Li atoms in Li_2S_2, Li_2S_4 and Li_2S_8 and adjacent F atoms in Ti_2CF_2 adsorption configurations. **d–f** The charge transfers between S/Li atoms and adjacent N atoms in NG adsorption configurations.

perpendicular direction. The characteristics of anisotropic polarizability can be simply estimated by atomic polarizability matrix, which exhibits both spatial distributions and orientations of the polarizability in LiPSs cluster. For Li_2S_4 adsorbed on Ti_2CF_2 in Supplementary Fig. 5, the polarizability matrixes show different anisotropic characteristics and the xy-orientational polarizability is much larger than that of Li_2S_6 and Li_2S_8, consistent with the optimized adsorption structures. Figure 2a shows that the Li_2S, Li_2S_2, and Li_2S_4 species "stand" on the surface with two Li atoms parallel to the surface of Ti_2CF_2, along with a charge transfer of 0.73–1.08 e. For Li_2S_6 and Li_2S_8, however, the configurations transform to "lying-in-plane" configuration, with only one Li atom binding with Ti_2CF_2, and a decreased charge transfer (0.42 e for Li_2S_6 and 0.58 e for Li_2S_8).

In light of the charge distribution analysis[41] shown in Fig. 3, we find that all F atoms in the F-terminated surface have a negative charge of 0.75 e. As for NG, N atoms obtain a large charge of 1.2 e, but other C atoms are nearly electroneutral. Since the vdW forces arise from the electrostatic interactions between the constantly fluctuating electron clouds, the spontaneous polarization in Ti_2CF_2 make the polarizability sensitive to electron exchange. The above analysis shows that reduction of electron transfer is probably the major reason that causes the sharply reduction of the $\Delta\alpha_{\perp}$. Meanwhile, from the density of states (DOS) of NG and Ti_2CF_2 (Supplementary Fig. 6) we find that they maintained its metallic properties after adsorption of Li_2S_6, implying that they can supply electrons directly to the redox reaction of the anchored LiPSs. To further understand the many-body effect in MXene systems, we calculated the anchoring behavior of $Ti_3C_2F_2$ (Supplementary Table 4), which was also applied as an anchoring material in Li–S batteries.[42] Compared with five atomic-layer Ti_2CF_2, we find that the polarizability perpendicular to plane ($\Delta\alpha_{\perp}$) and the ratio of MBD contribution (R_{MBD}) are both enhanced with the increasing thickness of anchoring materials.

From the above analysis, we find that Ti_2CF_2 systems has large polarization (22.2–41.3 bohr^3) and adsorption of LiPSs is dominated by the vdW interactions, which generates stronger many-body effect (large R_{MBD}). We also investigate other 2D materials such as TiS_2, Ti_2CO_2,[43,44] and $Ti_3C_2F_2$[20,28] and the binding energies from two methods (PBE + vdW^{surf} and PBE + MBD) are listed in Supplementary Table 5. We find that the many-body effect also exists in these systems. Therefore, for this type of anchoring materials with large R_{MBD}, pairwise-vdW methods tend to overestimate the anchoring performance (ΔE) even get an inverse conclusion of anchoring materials. Conversely, chemical bonding plays an important role during the whole process of lithiation in NG systems, and NG has a small polarization (4.3–12 bohr^3). As such, R_{MBD} is very small and pairwise-vdW and MBD method have the same prediction about ΔE.

In Li–S batteries, the adsorption of LiPSs on loading materials or solvent molecules is a process of competition, thus positive ΔE is the prerequisite for the anchoring materials.[4] It is clearly seen that NG has a large ΔE, which agrees with the experimental results that NG can effectively anchor lithium polysulfides. However, the limited number of adsorption sites discourages high energy density of sulfur cathodes. In addition, the ΔE of Li_2S_6 is as small as 0.02 eV, which demonstrates that Ti_2CF_2 would not effectively trap Li_2S_6 species, and the desorption and dissolution of Li_2S_6 species has a high probability to take place during lithiation.

DISCUSSION

We find the many-body dispersion interaction has a substantial impact on anchoring mechanism through binding energies of adsorption systems, especially for Ti_2CF_2 with strong polarization. According to the anchoring factor ΔE from the PBE + MBD method, we theoretically predict that Li_2S_6 partly dissolves into electrolytes solution and the DME/DOL solution with Li_2S_6 discolors incompletely when FeS and SnS_2 as anchoring materials, which agree well with the experiment. We demonstrated that the MBD approach can accurate predict the anisotropic polarizability and the anchoring behavior in the Li–S batteries. By systematically investigating the many-body effect on Ti_2CF_2 and NG systems, we found that the PBE + MBD method reduces the E^{b}_{AM} over 20%, as compared to the PBE + vdW^{surf} method at high-order lithiation stages for Ti_2CF_2 systems. While for NG systems, the energy difference from two methods is slight. Our work deepens the understanding of the anchoring mechanism, and provides a more accurate criterion for screening anchoring materials to control shuttle effect and to design more reliable cathode in Li–S batteries.

METHODS

Computational details

Our density functional theory (DFT) calculations were performed using the Fritz-Haber-Institute ab initio molecular simulations (FHI-aims) package[45] and the Vienna Ab initio Simulation Package (VASP) code.[46,47] The geometric optimization and the calculations of the charge transfer were performed within the generalized gradient approximation (GGA) of the Perdew-Burke-Ernzerhof (PBE) as implemented in VASP. For geometric optimizations, all atomic positions were relaxed until the maximal forces per atom were less than 0.03 eV/Å and energy difference was smaller than 10^{-5} eV. The plane-wave cutoff energy was set to 450 eV. A 3 × 3 supercell of monolayer FeS (SnS_2), a 5 × 5 supercell of Ti_2CF_2 with 5 × 5 × 1

Γ-centered *k*-mesh,[48] and a 7×7 supercell of NG with $3 \times 3 \times 1$ Γ-centered k-mesh were employed to model the adsorption systems. The distance of vacuum region was set to 20 Å along the z-direction (vertical to the interface) to avoid the interaction between adjacent layers.[49]

The FHI-aims code was applied to calculate density of states and energies of all configurations. We used the "tight" settings for numerical atom-centered orbital basis sets. The "tier2" standard basis was utilized for F, O, H, N, Li and C, and "tier1" for S, Fe, Ti, and Sn. The convergence criteria of 10^{-5} electrons per unit volume for the charge density and 10^{-6} eV for the total energy of the systems were used.

Van der Waals inclusive methods

For the description of the van der Waals (vdW) interactions we applied two methods in DFT calculations. The PBE + vdW^{surf} method[50] were employed to account for the pairwise van der Waals (vdW) interactions. The PBE + vdW^{surf} total energy includes the dispersion energy by considering a sum of $-C_6^{ab}R_{ab}^{-6}$ terms, where R_{ab} is the distance between atoms *a* and *b*, the C_6 coefficients and vdW radii (vdW parameters) are determined by the collective screening of the substrate electrons, which are captured by mean of the vdW^{surf} method. We employed the PBE + MBD method to describe the many-body dispersion (MBD) effect. The MBD method computes the correlation energy of long-range electrostatic screening through the coupled harmonic oscillator model Hamiltonian, and considers dipolar vdW interactions to all orders (many-body effect) in perturbation theory beyond the vdW^{surf} method.

DATA AVAILABILITY

The data supporting the findings of this study are available from the corresponding author on reasonable request.

Received: 27 July 2019; Accepted: 3 January 2020;
Published online: 30 January 2020

REFERENCES

1. Crabtree, G. Perspective The energy-storage revolution. *Nature* **526**, S92 (2015).
2. Manthiram, A., Chung, S. H. & Zu, C. Lithium-sulfur batteries: progress and prospects. *Adv. Mater.* **27**, 1980–2006 (2015).
3. Bruce, P. G., Freunberger, S. A., Hardwick, L. J. & Tarascon, J. M. Li-O_2 and Li-S batteries with high energy storage. *Nat. Mater.* **11**, 19–29 (2011).
4. Yang, Y., Zheng, G. & Cui, Y. Nanostructured sulfur cathodes. *Chem. Soc. Rev.* **42**, 3018–3032 (2013).
5. Evers, S. & Nazar, L. F. New approaches for high energy density lithium–sulfur battery cathodes. *Acc. Chem. Res.* **46**, 1135–1143 (2013).
6. Liang, Z., Qu, C., Guo, W., Zou, R. & Xu, Q. Pristine metal-organic frameworks and their composites for energy storage and conversion. *Adv. Mater.* **30**, e1702891 (2018).
7. Chung, W. J. et al. The use of elemental sulfur as an alternative feedstock for polymeric materials. *Nat. Chem.* **5**, 518–524 (2013).
8. Siczek, K. J. *Next-generation Batteries with Sulfur Cathodes*. (Academic Press, 2019).
9. Manthiram, A., Fu, Y. & Su, Y.-S. Challenges and prospects of lithium–sulfur batteries. *Acc. Chem. Res.* **46**, 1125–1134 (2013).
10. Ji, X., Lee, K. T. & Nazar, L. F. A highly ordered nanostructured carbon-sulphur cathode for lithium-sulphur batteries. *Nat. Mater.* **8**, 500–506 (2009).
11. Song, J. et al. Nitrogen-doped mesoporous carbon promoted chemical adsorption of sulfur and fabrication of high-areal-capacity sulfur cathode with exceptional cycling stability for lithium-sulfur batteries. *Adv. Funct. Mater.* **24**, 1243–1250 (2014).
12. Tao, X. et al. Balancing surface adsorption and diffusion of lithium-polysulfides on nonconductive oxides for lithium-sulfur battery design. *Nat. Commun.* **7**, 11203 (2016).
13. Li, Z. et al. A sulfur host based on titanium monoxide@carbon hollow spheres for advanced lithium-sulfur batteries. *Nat. Commun.* **7**, 13065 (2016).
14. Hu, L. et al. A highly efficient double-hierarchical sulfur host for advanced lithium-sulfur batteries. *Chem. Sci.* **9**, 666–675 (2018).
15. Li, C. et al. Titanium nitride hollow nanospheres with strong lithium polysulfide chemisorption as sulfur hosts for advanced lithium-sulfur batteries. *Nano Res.* **11**, 4302–4312 (2018).
16. Naguib, M. et al. Two-dimensional transition metal carbides. *ACS Nano* **6**, 1322–1331 (2012).
17. Xie, Y. et al. Role of surface structure on Li-ion energy storage capacity of two-dimensional transition-metal carbides. *J. Am. Chem. Soc.* **136**, 6385–6394 (2014).
18. Mashtalir, O., Lukatskaya, M. R., Zhao, M. Q., Barsoum, M. W. & Gogotsi, Y. Amine-assisted delamination of Nb_2C MXene for Li-ion energy storage devices. *Adv. Mater.* **27**, 3501–3506 (2015).
19. Luo, J. et al. Pillared structure design of mxene with ultralarge interlayer spacing for high-performance lithium-ion capacitors. *ACS Nano* **11**, 2459–2469 (2017).
20. Xiong, D., Li, X., Bai, Z. & Lu, S. Recent advances in layered $Ti_3C_2T_x$ MXene for electrochemical energy storage. *Small* **14**, e1703419 (2018).
21. Anasori, B., Lukatskaya, M. R. & Gogotsi, Y. 2D metal carbides and nitrides (MXenes) for energy storage. *Nat. Rev. Mater.* **2**, 16098 (2017).
22. Song, J. et al. Immobilizing polysulfides with mxene-functionalized separators for stable lithium-sulfur batteries. *ACS Appl. Mater. Interfaces* **8**, 29427–29433 (2016).
23. Zhou, F. et al. Low cost metal carbide nanocrystals as binding and electrocatalytic sites for high performance Li-S batteries. *Nano. Lett.* **18**, 1035–1043 (2018).
24. Bao, W. et al. Facile synthesis of crumpled nitrogen-doped MXene nanosheets as a new sulfur host for lithium-sulfur batteries. *Adv. Energy Mater.* **8**, 1702485 (2018).
25. Wang, H., Zhang, W., Xu, J. & Guo, Z. Advances in polar materials for lithium-sulfur batteries. *Adv. Funct. Mater.* **28**, 1707520 (2018).
26. Hou, T. Z. et al. Design principles for heteroatom-doped nanocarbon to achieve strong anchoring of polysulfides for lithium-sulfur batteries. *Small* **12**, 3283–3291 (2016).
27. Zhang, Q. et al. Understanding the anchoring effect of two-dimensional layered materials for lithium-sulfur batteries. *Nano Lett.* **15**, 3780–3786 (2015).
28. Zhou, G. et al. Catalytic oxidation of Li_2S on the surface of metal sulfides for Li-S batteries. *Proc. Natl Acad. Sci. USA* **114**, 840–845 (2017).
29. Sim, E. S., Yi, G. S., Je, M., Lee, Y. & Chung, Y.-C. Understanding the anchoring behavior of titanium carbide-based MXenes depending on the functional group in Li-S batteries: A density functional theory study. *J. Power Sources* **342**, 64–69 (2017).
30. Yin, L.-C. et al. Understanding the interactions between lithium polysulfides and N-doped graphene using density functional theory calculations. *Nano Energy* **25**, 203–210 (2016).
31. Brandenburg, J. G. et al. Physisorption of water on graphene: subchemical accuracy from many-body electronic structure methods. *J. Phys. Chem. Lett.* **10**, 358–368 (2019).
32. Yang, S., Jiang, Y., Li, S. & Liu, W. Many-body dispersion effects on the binding of TCNQ and F4-TCNQ with graphene. *Carbon* **111**, 513–518 (2017).
33. Maurer, R. J., Ruiz, V. G. & Tkatchenko, A. Many-body dispersion effects in the binding of adsorbates on metal surfaces. *J. Chem. Phys.* **143**, 102808 (2015).
34. Liu, W. et al. Quantitative prediction of molecular adsorption: structure and binding of benzene on coinage metals. *Phys. Rev. Lett.* **115**, 036104 (2015).
35. Qiu, Y. et al. High-rate, ultralong cycle-life lithium/sulfur batteries enabled by nitrogen-doped graphene. *Nano Lett.* **14**, 4821–4827 (2014).
36. Zhang, H. et al. Designing flexible 2D transition metal carbides with strain-controllable lithium storage. *Proc. Natl Acad. Sci. USA* **114**, E11082–E11091 (2017).
37. Fu, Z. et al. Mechanistic quantification of thermodynamic stability and mechanical strength for two-dimensional transition-metal carbides. *J. Phys. Chem. C* **122**, 4710–4722 (2018).
38. Kamphaus, E. P. & Balbuena, P. B. First-principles investigation of lithium polysulfide structure and behavior in solution. *J. Phys. Chem. C.* **121**, 21105–21117 (2017).
39. Ambrosetti, A., Ferri, N., DiStasio, R. A. & Tkatchenko, A. Wavelike charge density fluctuations and van der Waals interactions at the nanoscale. *Science* **351**, 1171 (2016).
40. Tkatchenko, A., DiStasio, R. A. Jr., Car, R. & Scheffler, M. Accurate and efficient method for many-body van der Waals interactions. *Phys. Rev. Lett.* **108**, 236402 (2012).
41. Bader, R. *Atoms in Molecules-A Quantum Theory*. (Oxford University, 1990).
42. Wang, D. et al. A general atomic surface modification strategy for improving anchoring and electrocatalysis behavior of $Ti_3C_2T_2$ MXene in lithium-sulfur batteries. *ACS Nano* **13**, 11078–11086 (2019).
43. Chen, S. et al. Surface electrochemical stability and strain-tunable lithium storage of highly flexible 2D transition metal carbides. *Adv. Funct. Mater.* **28**, 1804867 (2018).
44. Ibragimova, R., Puska, M. J. & Komsa, H. P. pH-dependent distribution of functional groups on titanium-based MXenes. *ACS Nano* **13**, 9171–9181 (2019).
45. Blum, V. et al. Ab initio molecular simulations with numeric atom-centered orbitals. *Comput. Phys. Commun.* **180**, 2175–2196 (2009).
46. Kresse, G. & Furthmüller, J. Efficiency of ab-initio total energy calculations for metals and semiconductors using a plane-wave basis set. *Comput. Mater. Sci.* **6**, 15–50 (1996).

47. Kresse, G. & Furthmüller, J. Efficient iterative schemes for ab initio total-energy calculations using a plane-wave basis set. *Phys. Rev. B* **54**, 11169–11186 (1996).
48. Monkhorst, H. J. & Pack, J. D. Special points for Brillouin-zone integrations. *Phys. Rev. B* **13**, 5188–5192 (1976).
49. Liu, W., Tkatchenko, A. & Scheffler, M. Modeling adsorption and reactions of organic molecules at metal surfaces. *Acc. Chem. Res.* **47**, 3369–3377 (2014).
50. Ruiz, V. G., Liu, W., Zojer, E., Scheffler, M. & Tkatchenko, A. Density-Functional Theory with Screened van der Waals Interactions for the Modeling of Hybrid Inorganic-Organic Systems. *Phys. Rev. Lett.* **108**, 146103 (2012).

ACKNOWLEDGEMENTS

We acknowledge supports from the NSF of China (51602155, 51722102, 21773120), the NSF of Jiangsu Province (BK20180448), the Fundamental Research Funds for the Central Universities (30918011340, 30919011405, 30917011201) and Jiangsu Key Laboratory of Advanced Micro&Nano Materials and Technology.

AUTHOR CONTRIBUTIONS

S.L. and W.L. directed and designed the whole research. M.F. did all calculations and wrote the manuscript. All authors discussed the results and provided inputs to the manuscript.

COMPETING INTERESTS

The authors declare no competing interests.

ADDITIONAL INFORMATION

Supplementary information is available for this paper at https://doi.org/10.1038/s41524-020-0273-1.

Correspondence and requests for materials should be addressed to S.L. or W.L.

Reprints and permission information is available at http://www.nature.com/reprints

Publisher's note Springer Nature remains neutral with regard to jurisdictional claims in published maps and institutional affiliations.